

UNCALIBRATED CAMERA IMAGES IN DELINEATING PARCEL BOUNDARIES

Oliver T. Macapinlac

Assistant Professor, Department of Geodetic Engineering,
University of the Philippines Diliman, Quezon City, Philippines 1101
Email: otmacapinlac@up.edu.ph

ABSTRACT

The reconstruction of 3D points from two view camera images has found several applications in various fields of engineering, science and architecture today. Many of these fields are involved in the generation of 3D models using diverse technology in 3D reconstruction. In geomatics, estimating 2D or 3D locations can be made through direct or indirect measurement. Direct measurements involve laser technology (e.g. total stations), satellite positioning and terrestrial laser scanning. Indirect methods, on the other hand, involve remote sensing, aerial and terrestrial photogrammetry. In delineating parcel boundaries, direct measurements with total stations and global navigation satellite systems (GNSS) are used in field operations. Although these have been quite stable with satisfactory results, the cost of operations is still relatively higher compared to indirect measurements, especially in larger areas of coverage. This study investigated the feasibility of using close-range photogrammetry thru uncalibrated image pairs for fast acquisition of target locations. The general algorithm will derive the fundamental matrix, generate the camera matrices, triangulate the projective 3D positions and finally transform these points to their metric ground 3D positions using Ground Control Points (GCP). The extracted northing (y-coordinates) and easting (x-coordinates) of the parcel's corners were compared to coordinates derived from total stations. These showed an error vector of up to 10 cm. Results also revealed that the required accuracy for tertiary survey can be achieved around 30 percent distance from the image center. Beyond this, the positional error increases, making this method unsuitable for boundary delineation. The RMSE of this set of points was 0.0758 m or 7.58 cm.

Key Words: *Close Range Photogrammetry, Computer Vision, 3D Reconstruction, Direct Linear Transformation*

1. INTRODUCTION

Geographic information (GI) and its utilization are starting to gain wide acceptance in day to day activities due to technologies like the web and mobile Geographic Information System (GIS). Combined with Global Navigation Satellite System (GNSS), GI becomes an indispensable tool for navigation and query that captures a handful of devices for implementation. The key to this level of technology can be attributed to several factors: hardware becoming powerful yet affordable; software and techniques becoming complex and optimized; and data becoming more available and detailed at least for mapping. Spatial data-capturing technology developed and evolved in the last few decades from analogue to fully digital. The challenge in this rapid development in GI applications is the incorporation of spatial data that is at par with direct land survey in accuracy and precision.

Cadastral survey is a form of land survey which aims to speed up the land registration procedure of every parcel of lot in a municipality. In the Philippines, the technical aspect of the cadastral survey consists of surveying activities such as project control surveys, political boundary surveys and lot surveys (DENR, 2007). Allowable positional errors when conducting the lot survey usually do not exceed ± 10 centimeters, or the difference in area not exceeding ± 1 square meter for every hectare of parcel (DENR, 2007). As of 2010, the approved cadastral survey has reached 52.3% (17,946,889 has. of 34,328,203 has.) of the total land area that should be covered by cadastral survey activities (LMB, 2011).

Ground surveying is indisputably the best procedure in building highly accurate and precise spatial data. However, the identification of lot boundaries thru ground surveying techniques is time-consuming and expensive. Updating parcel data is even more challenging in urban areas as the configuration of spatial data is complicated, and direct measurement is difficult due to inaccessibility. In addition, the increasing demand for spatial data in many GI applications tends to require alternative methods of acquisition.

For decades, one of the main alternatives in building spatial data is *photogrammetry*. Aerial photogrammetry measures ground features and physical dimensions from vertically oriented photo images captured from platforms inside the atmosphere (e.g. airplanes and balloons). When the images are acquired near or on the surface of the earth, providing finer dimensional information of the ground feature, the method becomes classified as terrestrial photogrammetry. Further reducing the camera-to-object distance to around 100 m or less, terrestrial photogrammetry is classified as close-range photogrammetry (Jiang, Jauregui, & White, 2008). This method of photogrammetric acquisition of object features is characterized by processing highly convergent camera alignment and orientation. The International Society of Photogrammetry and Remote Sensing (ISPRS) Commission V: Close-Range Sensing: Analysis and Applications accounts several research and applications of this field, together with machine and computer visions (ISPRS, 2011).

Uncalibrated Euclidean reconstruction was explored in this study to address the challenge of building spatial data that is as precise as ground survey but uses minimal time and effort. In close range photogrammetry and computer vision, there are two approaches to estimate the 3D information of ground objects.

The first approach works by deriving the camera-to-ground model based on an initial camera calibration process. There are two sets of camera parameters in this model—the intrinsic and extrinsic camera values for estimation. The Intrinsic model estimates the internal geometry and the optical characteristic of the camera, while the Extrinsic parameter relates the camera to the world coordinate system thru the measurement of the position and orientation of the imaging system.

In the last few years, there had been various techniques devised to deal with camera calibration. A study was conducted to review some of the most frequently used calibration

techniques by comparing their nomenclature and notation, as well as the accuracy of each method (Salvi, Armangué, & Batlle, 2002). Once calibration is achieved, the camera model is used to compute the 3D position of the object by triangulating at least two optical rays derived from images. Although the step towards reconstructing full metric information of ground features is through these calibration techniques, some situations will need to explore the uncalibrated case (Fusiello, 2000). In such instance, the intrinsic and extrinsic parameters are unknown or are not derived because calibration is not deemed practical. For example, the movement of the camera to a general position due to inaccessibility of ground target could pose difficulty in the calibrated approach.

The second approach is based on the premise that calibration cannot be achieved. This approach describes the epipolar geometry between two-view images and estimates the fundamental matrix which is the algebraic representation of the epipolar geometry (Hartley & Zisserman, 2003). The topic of estimating fundamental matrix is a research in its own right. Several techniques from these researches became the basis for many commercial software such as PhotoModeler (EOS Systems Inc., 2012) and ImageModeler (Autodesk Inc, 2012), as well as open source software such as insight3d (insight3d, 2009).

Techniques in estimating the fundamental matrix were broadly classified as linear, iterative or robust method. Linear methods are quite good if the point correspondences are well located in the image pair; iterative methods can cope with noise; and robust methods are well-suited for correspondences with outliers (Armangué & Salvi, 2003).

Estimating the fundamental matrix from point correspondences is just the first step in 3D Euclidean reconstruction. A major achievement of the uncalibrated approach is the reconstruction up to a projective transformation. Studies show that auto calibration and stratification were some of the most common approaches in achieving 3D Euclidean reconstruction (Fusiello, 2000). Hartley et al also made a concise discussion of the stratified approach where reconstruction begins with a projective reconstruction, then refined progressively to an affine and eventually to a metric (similarity) reconstruction. They also established that the availability of ground control point makes a direct method to Euclidean reconstruction possible without traversing the stratified method (Hartley & Zisserman, 2003). This approach was applied to underwater images as well as in employing additional information from the scene as ground truth (Plakas & Trucco, 1998).

This research aims to apply the procedures in uncalibrated 3D reconstruction with ground control points to extract the horizontal position of a parcel of land. It also provides an overview of current land surveying processes in delineating parcel boundaries, while developing an alternative field operation using 3D reconstruction. An experiment was conducted wherein parcels of lots were located through conventional surveying procedures using GNSS for control and total station for parcel boundary delineation. Images of the same parcels were then captured using off-the-shelf digital SLR camera. These were processed and the coordinates of the boundaries extracted using the uncalibrated approach. Finally, the accuracy of the experiment was compared to actual processed position derived from a conventional land surveying method.

2. BASIC CONCEPT AND NOTATION

This section will discuss the basic notation and mathematical background of the uncalibrated reconstruction approach used in the study. Notation and algorithm follows that of Hartley & Zisserman (2003).

2.1 Projective geometry and the camera geometry

An image is the 2D representation of a 3D world. The drop from 3D world to a 2D image is a projection process in which a ray from a point on the 3D world plane is drawn through a fixed point in space to the 2D image plane. Fig. 1 illustrates the central projection process in which point C is the center of projection of the rays. A pinhole camera has the same concept as this model in which the ray of light from a point in the world passes through the camera lens and is captured on the digital image device.

The mathematics of the imaging process is based on projective geometry. In this geometry, the world is described in terms of the 3D projective space P^3 and the image measured in 2D projective space P^2 . The imaging process is therefore a mapping or transformation from P^3 to P^2 .

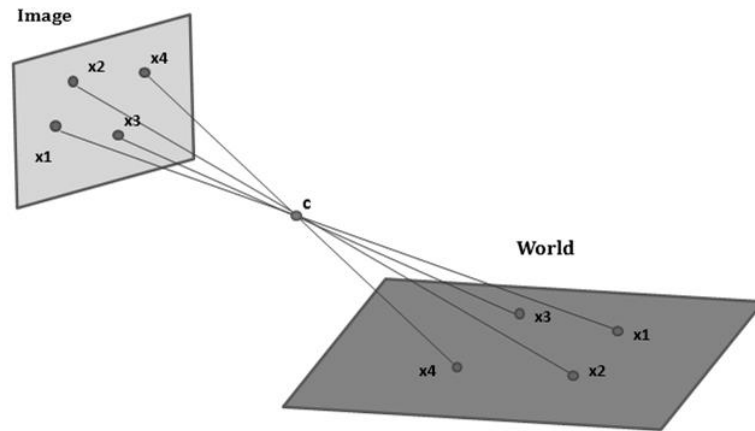


Fig. 1 World to image projection

The homogeneous (or projective) coordinates of the image x and world \mathbf{X} is

$$x = \begin{bmatrix} x \\ y \\ w \end{bmatrix} \quad \mathbf{X} = \begin{bmatrix} X \\ Y \\ Z \\ T \end{bmatrix}$$

and the transformation from the \mathbf{X} to x is given by the matrix operation

$$\begin{bmatrix} x \\ y \\ w \end{bmatrix} = P_{3 \times 4} \begin{bmatrix} X \\ Y \\ Z \\ T \end{bmatrix}$$

where $P_{3 \times 4}$ is the simple camera matrix which is modeled by a perspective projection matrix.

The camera matrix P can further be decomposed, using QR factorization into the form $P = K[R|t]$. K describes the calibration matrix or the intrinsic parameters of the camera and usually of the form

$$K = \begin{bmatrix} \alpha_x & s & x_0 \\ 0 & \alpha_y & y_0 \\ 0 & 0 & 1 \end{bmatrix}$$

where $\alpha_x = fm_x$ and $\alpha_y = fm_y$ represent the focal length of the camera in horizontal m_x and vertical m_y pixels. Similarly, x_0 and y_0 is the principal point in terms of pixel dimensions with coordinates $x_0 = p_x m_x$ and $y_0 = p_y m_y$. The s in the matrix is referred to as skew parameter in a general projective camera.

The matrix R and t describe the position and orientation or the extrinsic parameters of the camera. These are necessary to transform the camera reference frame to the world reference frame (see Fig. 1).

From the matrix formula, it is relatively straightforward to reconstruct the 3D world if the camera matrix P (with the intrinsic and extrinsic parameter supplied) is known. However, for the uncalibrated case, these parameters are not available.

2.2 Epipolar geometry and the fundamental matrix

As calibration is not possible in the uncalibrated approach, the intrinsic and extrinsic camera parameters are derived using other means. Intrinsic parameters can be derived from the epipolar geometry between two views. Fig. 2 shows the projective camera geometry between two views capturing the same world.

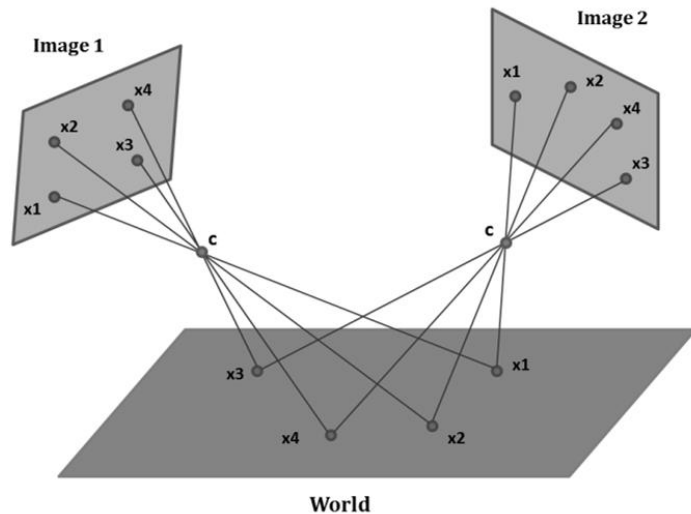


Fig. 2 Cameras capturing the same world

The epipolar geometry is simply the geometry of the epipoles and epipolar line which is essentially the intersection of the image planes with a plane created from camera centers of the two images and the world point. Fig. 3 shows the epipoles, epipolar lines and epipolar plane.

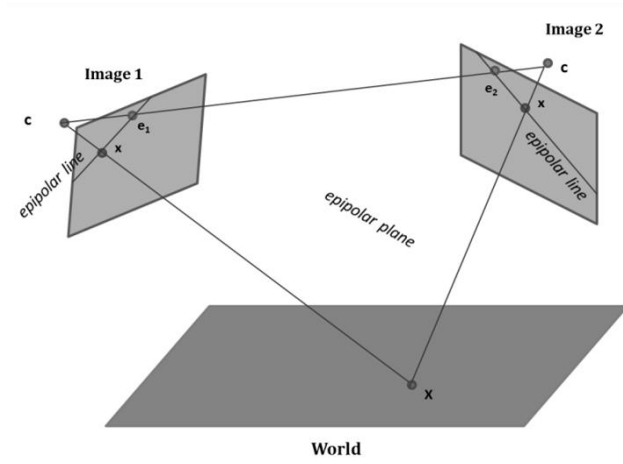


Fig. 3 Epipolar geometry showing a single epipolar plane

This geometry can be derived by determining or searching for sets of point correspondences x and x' in both images. Epipole e is the intersection of the line defined by the camera centers c with the image plane. One can deduce that all the epipolar lines generated by all the point correspondences will meet at the epipole.

The algebraic representation of the epipolar geometry is the fundamental matrix. Its geometric derivation constitutes two steps: the point transfer via epipolar plane and the construction of the epipolarline. Fig. 4 shows a ray through point x in the left image meeting with the point X in the world plane. The point X is then projected to point x' in the second image.

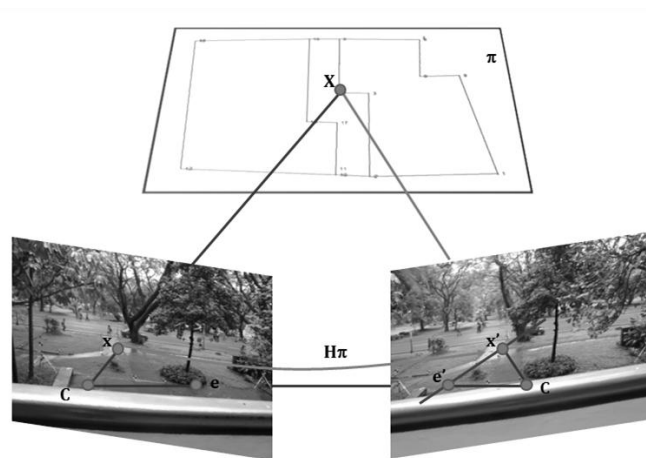


Fig. 4 Point transfer from image 1 to image 2

It can be written that

$$x' = H_{\pi}x$$

which shows that the set of all point x in the first image is a 2D homography H_{π} mapping to the corresponding point x' in the second image.

Since all the three points x , x' and X are lying on the same plane (epipolar plane), the projected point x' in the second image must lie on the epipolar line l' of that image. This can be written as

$$l' = e' \times x' = [e']_{\times}x'$$

and substituting $x' = H_{\pi}x$, we have

$$l' = [e']_{\times}H_{\pi}x = Fx$$

and

$$F = [e']_{\times}H_{\pi}$$

From this geometry, it can be shown that for each point x in one image, there exists a corresponding epipolar line l' in the other image. This mapping of point to the epipolar line $x \rightarrow l'$

is a projective mapping which is represented by a matrix F , the fundamental matrix.

Bearing in mind that the back-projection of image point x to world point X is obtained by solving $PX = x$, (Hartley & Zisserman, 2003) shows the derivation of the fundamental matrix in the form

$$F = [e']_{\times}P'P^{+}$$

in which P^{+} is the pseudo-inverse of P . This shows that the fundamental matrix can be derived in terms of the two camera projective matrices P and P' .

One of the important concepts of the fundamental matrix is the correspondence condition which states that for any pair of corresponding points $x \leftrightarrow x'$ in the two images, x' lies on the epipolar line l' . This can be expressed with the product: $0 = x'^T l'$. With $l' = Fx$, the form becomes

$$x'^T Fx = 0$$

Epipolar geometry is independent of the scene structure and can be computed from the corresponding points x and x' of the two images only, and without initial knowledge of the camera's internal parameters. Furthermore, it can be seen from Fig. 4 that a choice of world frame, for instance changing the plane π , will affect the camera matrix P and P' but not the fundamental matrix F .

2.3 Fundamental matrix and the camera matrix

The camera matrices P and P' uniquely determine the fundamental matrix. The opposite is not true. If we take the first camera reference frame as the world reference frame, the first camera matrix in its simplest form (canonical form) is

$$P = [I|0]$$

where I is a 3×3 identity matrix. It can be shown that the second camera matrix will be of the form

$$P' = [[e']_{\times}F|e']$$

Further deriving the matrix expression, the general formula (Hartley & Zisserman, 2003) for a pair of canonic camera matrices in terms of the fundamental matrix is given by

$$P = [I|0]$$

and

$$P' = [[e']_x F + e'v^T | \lambda e']$$

where v is any 3-vector for instance $\begin{bmatrix} 1 \\ 1 \\ 1 \end{bmatrix}$, and λ a non-zero scalar such as 1.

2.4 Linear triangulation and DLT

Given enough point correspondences between the two images, the fundamental matrix F and the canonic camera matrices P and P' can be computed uniquely. For each point correspondence $x \leftrightarrow x'$, the point \mathbf{X} in world space that projects to these two image points can be computed by

$$x_i = P\mathbf{X}_i$$

and

$$x'_i = P'\mathbf{X}'_i$$

Since the measured point correspondences $x \leftrightarrow x'$ contain errors, there will be no point \mathbf{X} in the world space that would satisfy the above equations. The solution is the composition of a triangulation method

$$\mathbf{X} = \tau(x, x', P, P')$$

that could compute the 3D point \mathbf{X} from the point correspondences $x \leftrightarrow x'$ and the camera matrices P and P' . Given that in each image, there are $x_i = P\mathbf{X}_i$ and $x'_i = P'\mathbf{X}'_i$, the cross product, $x \times P\mathbf{X} = 0$ will yield two independent equations, linear in the component of \mathbf{X} :

$$x(p^{3T}\mathbf{X}) - (p^{1T}\mathbf{X}) = 0$$

$$y(p^{3T}\mathbf{X}) - (p^{2T}\mathbf{X}) = 0$$

where p^{iT} are the rows of P .

Two equations included in each image will create this set of linear equations:

$$x(p^{3T}\mathbf{X}) - (p^{1T}\mathbf{X}) = 0$$

$$y(p^{3T}\mathbf{X}) - (p^{2T}\mathbf{X}) = 0$$

$$x'(p'^{3T}\mathbf{X}) - (p'^{1T}\mathbf{X}) = 0$$

$$y'(p'^{3T}\mathbf{X}) - (p'^{2T}\mathbf{X}) = 0$$

which has a general form $A\mathbf{X} = 0$. Specifically

$$A = \begin{bmatrix} xp^{3T} - p^{1T} \\ yp^{3T} - p^{2T} \\ x'p'^{3T} - p'^{1T} \\ y'p'^{3T} - p'^{2T} \end{bmatrix}$$

This is a homogeneous equation, and the least square solution of \mathbf{X} is the singular vector corresponding to the smallest singular value of A (Hartley & Zisserman, 2003).

2.5 3D DLT: Projective to Euclidean reconstruction

The main goal of our application is to eventually arrive at a Euclidean or true reconstruction of the ground target. With the intrinsic (camera calibration) and extrinsic (position and orientation) models of the cameras unknown, reconstruction can only be achieved up to a projective transformation. However, using ground control points, it is possible for the projective reconstruction to be transformed into its Euclidean reconstruction. Furthermore, the projective reconstruction \mathbf{X} is related to the true reconstruction $\bar{\mathbf{X}}$ by a homography, that is

$$H\bar{\mathbf{X}}_i = \lambda\mathbf{X}_i, \quad i = 1, \dots, n$$

where λ is a scale factor and H is the 4×4 homography matrix.

It could be seen that the solution follows the direct linear transformation (DLT). Given these equations where a_{ij} are the elements of H

$$\begin{aligned} a_{11}\bar{\mathbf{X}} + a_{12}\bar{\mathbf{Y}} + a_{13}\bar{\mathbf{Z}} + a_{14} &= \lambda\mathbf{X} \\ a_{21}\bar{\mathbf{X}} + a_{22}\bar{\mathbf{Y}} + a_{23}\bar{\mathbf{Z}} + a_{24} &= \lambda\mathbf{Y} \\ a_{31}\bar{\mathbf{X}} + a_{32}\bar{\mathbf{Y}} + a_{33}\bar{\mathbf{Z}} + a_{34} &= \lambda\mathbf{Z} \\ a_{41}\bar{\mathbf{X}} + a_{42}\bar{\mathbf{Y}} + a_{43}\bar{\mathbf{Z}} + a_{44} &= \lambda\mathbf{T} \end{aligned}$$

Dividing the whole set of equation by the 4th row (4th equation in the set) eliminates the scale factor λ , thus

$$\begin{aligned} \frac{a_{11}\bar{\mathbf{X}} + a_{12}\bar{\mathbf{Y}} + a_{13}\bar{\mathbf{Z}} + a_{14}}{a_{41}\bar{\mathbf{X}} + a_{42}\bar{\mathbf{Y}} + a_{43}\bar{\mathbf{Z}} + a_{44}} &= \frac{\lambda\mathbf{X}}{\lambda\mathbf{T}} \\ \frac{a_{21}\bar{\mathbf{X}} + a_{22}\bar{\mathbf{Y}} + a_{23}\bar{\mathbf{Z}} + a_{24}}{a_{41}\bar{\mathbf{X}} + a_{42}\bar{\mathbf{Y}} + a_{43}\bar{\mathbf{Z}} + a_{44}} &= \frac{\lambda\mathbf{Y}}{\lambda\mathbf{T}} \\ \frac{a_{31}\bar{\mathbf{X}} + a_{32}\bar{\mathbf{Y}} + a_{33}\bar{\mathbf{Z}} + a_{34}}{a_{41}\bar{\mathbf{X}} + a_{42}\bar{\mathbf{Y}} + a_{43}\bar{\mathbf{Z}} + a_{44}} &= \frac{\lambda\mathbf{Z}}{\lambda\mathbf{T}} \end{aligned}$$

Multiplying each element of the left side of the equation by $\frac{1}{a_{44}}$ will reduce the unknowns to 15 parameters in terms of L , where $L_1 = \frac{a_{11}}{a_{44}}$, $L_2 = \frac{a_{12}}{a_{44}}$ and so on, and will yield a non-zero vector on the right side of the equation. Rearranging the system of linear equation, will have the form:

$$\begin{aligned} L_1\bar{\mathbf{X}} + L_2\bar{\mathbf{Y}} + L_3\bar{\mathbf{Z}} + L_4 &= \frac{\mathbf{X}}{\mathbf{T}} (L_{13}\bar{\mathbf{X}} + L_{14}\bar{\mathbf{Y}} + L_{15}\bar{\mathbf{Z}} + 1) \\ L_5\bar{\mathbf{X}} + L_6\bar{\mathbf{Y}} + L_7\bar{\mathbf{Z}} + L_8 &= \frac{\mathbf{Y}}{\mathbf{T}} (L_{13}\bar{\mathbf{X}} + L_{14}\bar{\mathbf{Y}} + L_{15}\bar{\mathbf{Z}} + 1) \\ L_9\bar{\mathbf{X}} + L_{10}\bar{\mathbf{Y}} + L_{11}\bar{\mathbf{Z}} + L_{12} &= \frac{\mathbf{Z}}{\mathbf{T}} (L_{13}\bar{\mathbf{X}} + L_{14}\bar{\mathbf{Y}} + L_{15}\bar{\mathbf{Z}} + 1) \end{aligned}$$

Substituting the following expressions to $\pi = \frac{\mathbf{X}}{\mathbf{T}}(-\bar{\mathbf{X}})$, $\rho = \frac{\mathbf{X}}{\mathbf{T}}(-\bar{\mathbf{Y}})$, $\sigma = \frac{\mathbf{X}}{\mathbf{T}}(-\bar{\mathbf{Z}})$, $\tau = \frac{\mathbf{Y}}{\mathbf{T}}(-\bar{\mathbf{X}})$, $v = \frac{\mathbf{Y}}{\mathbf{T}}(-\bar{\mathbf{Y}})$, $\varphi = \frac{\mathbf{Y}}{\mathbf{T}}(-\bar{\mathbf{Z}})$, $\chi = \frac{\mathbf{Z}}{\mathbf{T}}(-\bar{\mathbf{X}})$, $\psi = \frac{\mathbf{Z}}{\mathbf{T}}(-\bar{\mathbf{Y}})$, and $\omega = \frac{\mathbf{Z}}{\mathbf{T}}(-\bar{\mathbf{Z}})$; and expressing the matrix equation in the form $B\Delta = f$.

Specifically, the matrix B , Δ and f are:

$$B = \begin{bmatrix} \bar{X} & \bar{Y} & \bar{Z} & 1 & 0 & 0 & 0 & 0 & 0 & 0 & 0 & \pi & \rho & \sigma \\ 0 & 0 & 0 & 0 & \bar{X} & \bar{Y} & \bar{Z} & 1 & 0 & 0 & 0 & \tau & \upsilon & \varphi \\ 0 & 0 & 0 & 0 & 0 & 0 & 0 & 0 & \bar{X} & \bar{Y} & \bar{Z} & 1 & \chi & \psi & \omega \end{bmatrix}$$

$$\Delta = \begin{bmatrix} L_1 \\ \vdots \\ L_{15} \end{bmatrix}$$

$$f = \begin{bmatrix} X/T \\ Y/T \\ Z/T \end{bmatrix}$$

Each ground control points will generate the system of equation above, thus 5 or more GCP will solve a unique set of the unknown L . This can be solved using least squares.

3. FIELD SETUP AND COMPUTATION

3.1 Field setup

The experimental setup of the study was patterned after the field operation in land surveying. Instruments such as the total station and GNSS were used for the control stations. The control stations were fixed with respect to a standard world reference coordinate system such as the Philippine Reference System (PRS) of 1992. A transfer of coordinate is usually done from control station to parcel corner points by making another observation thru a total station. This transfer of coordinates is the basis for many surveying applications, and it utilizes several direct measurement devices.

In the experiment, special markers were used to pinpoint the exact location of control points and parcel points as shown in Fig. 5. These were carefully observed using a total station. The coordinates of these points served as the true value for comparison with the computed coordinates of the uncalibrated reconstruction approach.



Fig. 5 Point markers in the experiment

For the 3D reconstruction using ground truth to work, at least 5 ground control points (in which no 4 of the GCP are coplanar) are obtained and supplied to the 3D-DLT algorithm (Hartley & Zisserman, 2003). In the experiment, three of the control stations were retrofitted with markers as shown in Fig. 6. This setup creates the volume control (GCP in general 3D position) needed for the computation.



Fig. 6 Control markers in the experiment

Several images were captured using a Canon EOS 500D Digital SLR camera with its zoom and resolution levels set to maximum (15.1 megapixel). Two images that capture all the target markers were selected, and a total of 17 markers, including the 6 volume control points, were identified in each image.

3.2 *Algorithm and computations*

The general algorithm used to derive the 3D Euclidean reconstruction of the markers follows:

1. Semi-automated determination of point correspondences using region growing and centroid computation
2. Fundamental matrix computation using 8-point normalization
3. Refinement of the fundamental matrix thru Sampson distance approximation of geometric distance error
4. Canonical camera matrices estimation
5. Triangulation using direct linear transformation (DLT)
6. Direct euclidean (true) reconstruction using 3D-DLT computation

3D reconstruction usually starts with the determination of point correspondences either thru manual or fully automated (such as RANSAC) selection of these points. In the study, a semi-automatic method was used to determine the point correspondences from the two images. This method involved an additional image processing step that would semi-automatically select the point correspondences.

Fig. 7 shows the processing done to the image to convert the RGB-value pixel to a Boolean (1 or 0) value pixel. The region where the marker targets are located was then programmatically computed using region growing. These regions were used to estimate the centroid of the marker. The user will still need to carefully pick a location near the region of the marker for this to work. This was done in each image until all 17 point correspondences were chosen.

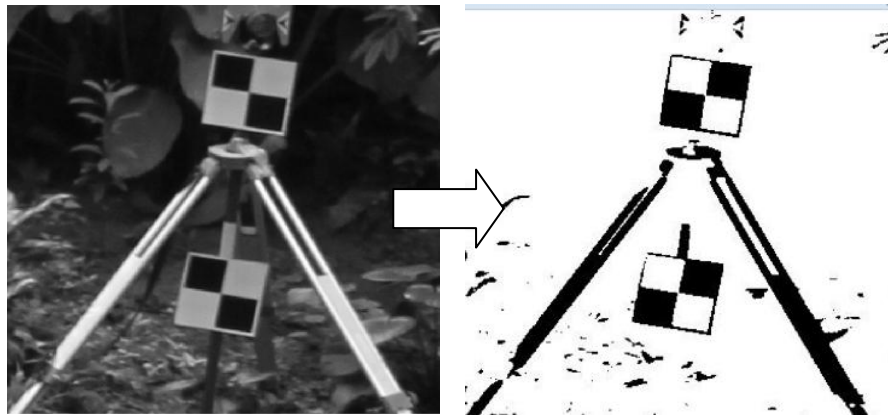


Fig. 7 Thresholding and region-growing

An initial estimate of the fundamental matrix was done using the normalized 8-point algorithm. To improve the initial estimate, it is necessary to minimize geometric distance error. Sampson approximation was used to provide a first-order approximation to the geometric error. Details of the algorithm were provided by Hartley & Zisserman (2003).

Following the computation of the fundamental matrix, the canonical camera matrices were derived and used to estimate the 3D reconstruction of the point correspondences. Hartley & Zisserman (2003) posed the triangulation computation (DLT) as solution, utilizing some matrix operations such as singular value decomposition (SVD). Java matrix libraries were used to implement the SVD computation.

Finally, the true reconstruction of the markers' locations was achieved thru a direct transformation from their computed projective coordinates. The 6-volume control points and their corresponding projective coordinates computed from triangulation were used to derive a homography H using 3D-DLT. The homography H effectively transforms each marker's projective coordinates to their Euclidean or true coordinates.

A java application was created to implement all the computations discussed above. Libraries such as Efficient Java Matrix Library (Abeles, Efficient Java Matrix Library, 2009) and BoofCV (Abeles, BoofCV, 2004) were included in the application. Several java classes were created to implement the algorithm. The output is a set of 3D coordinates (comma separated value, .csv file) of the markers that were plotted and analyzed using CAD and GIS.

4. RESULTS OF THE EXPERIMENT

The primary result of the study was a set of computed coordinates of the markers (corners) delineating the parcel boundaries. Thru direct transformation using 3D-DLT computation, these results were referred to the same reference frame of the coordinates extracted from ground

Table 1 shows the computed coordinates from the study and the coordinates from the total station.

Table 1 Measured and “true” coordinate of the markers

Marker	Uncalibrated		Land Surveying	
	N	E	N	E
1	19972.76	20011.90	19971.98	20012.53
2	19982.51	20010.37	19982.51	20010.57
3	19982.42	20007.63	19982.52	20007.63
4	19980.56	20004.09	19980.65	20004.04
5	19972.51	20003.95	19972.45	20003.96
6	19977.55	20001.95	19977.63	20001.93
7	19980.66	20002.05	19980.75	20002.02
8	19986.69	20002.10	19986.69	20002.06
9	19986.69	19999.98	19986.69	20000.00
10	19977.64	19999.96	19977.72	19999.97
11	19973.21	19992.24	19972.91	19992.12
GC1	19986.64	20007.87	19986.66	20007.86
GC2	19986.86	20007.78	19986.66	20007.86
GC3	19972.64	20001.87	19972.56	20001.87
GC4	19973.18	20001.86	19972.56	20001.85
GC5	19986.47	19991.81	19986.79	19992.03
GC6	19986.54	19991.85	19986.79	19992.02

The mean square error (MSE) in the x direction was 0.0787 m or 7.87 cm, while the MSE in the y direction was 0.0322 m or 3.22 cm. The locational accuracy (de By, 2001) or the root mean square error (RMSE) of the 17 markers was 0.332 m or 33.2 cm. Fig. 8 shows the positional errors at each point plotted as error vectors. It can be observed that as the point’s proximity increases from the center of the image, so does its error vector.

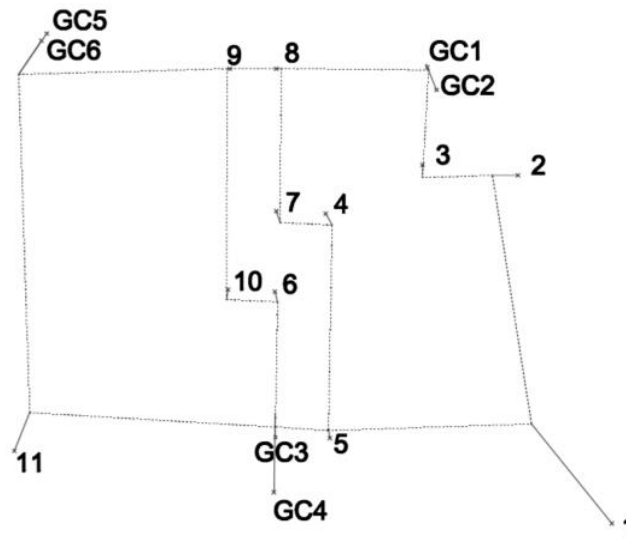


Fig. 8 Error vectors (solid lines) exaggerated 5x

In order to characterize this observation, the error vectors were plotted against their distance from the center of the image. This graph (Fig. 9) shows that point-correspondences within around 30% from the center of the image have errors of less than 10 cm.

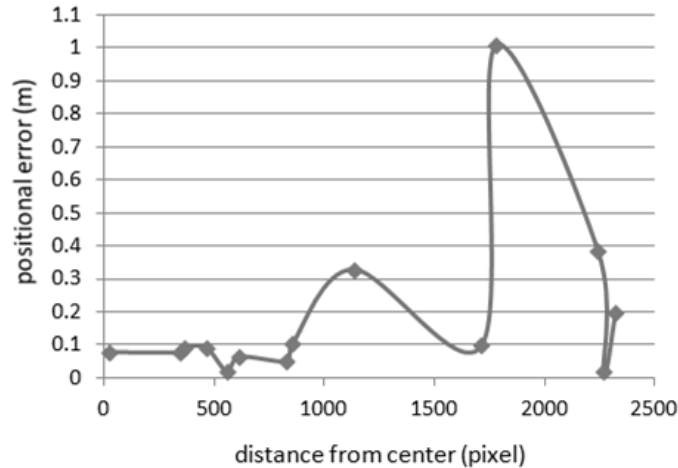


Fig. 9 Error vs Distance

A buffer was made to locate these points in the image. Point-correspondences within the buffer were identified to be of the lot delineating the concrete lane in the image (see Fig. 5 and Fig. 8). The RMSE and positional accuracy of this set of points was recomputed. Table 2 shows this set of points with their positional error. The MSE in the x direction was 0.0049 m or 0.49 cm, while the MSE in the y direction was 0.0009 m or 0.09 cm. The minimum error in position was 1.9 cm and the maximum was 10.5 cm. The locational accuracy or the root mean square error (RMSE) of this set was 0.0758 m or 7.58 cm.

Table 2 Points within the buffer zone

Marker	Uncalibrated		Land Surveying		Pos. Err (m)
	N	E	N	E	
5	19972.51	20003.95	19972.45	20003.96	0.063
GC3	19972.64	20001.87	19972.56	20001.87	0.076
6	19977.55	20001.95	19977.63	20001.93	0.090
10	19977.64	19999.96	19977.72	19999.97	0.077
9	19986.69	19999.98	19986.69	20000.00	0.019
8	19986.69	20002.10	19986.69	20002.06	0.050
7	19980.66	20002.05	19980.75	20002.02	0.092
4	19980.56	20004.09	19980.65	20004.04	0.105

5. DISCUSSION AND CONCLUSION

The study successfully evaluated the feasibility of the uncalibrated reconstruction approach in delineating boundaries of land parcels. However, the research showed that the entire image could not be used for reconstruction. This is because of the nature of the computation in which no calibration was done to the image. Although the intrinsic and extrinsic properties of the camera model were incorporated in the fundamental matrix and the 3D-DLT computations, the radial lens distortion is still present and unchecked. The results highlighted that the positional error vector can be minimized by confining the point correspondence to just the center of the image. Although correcting the radial distortion could increase the accuracy of the reconstruction, the study focused only on the raw data from the camera.

Ground survey is undisputedly the best method to extract position on the ground; however, the most important contribution of the study is the automatic reconstruction and extraction of positions with minimal human interactions. The positional accuracy (RMSE) of this approach can be comparable and acceptable to boundary delineation if the distance constraints were considered.

The study also shows the potential of close range photogrammetry and the uncalibrated reconstruction approach as an alternative to conventional ground surveying practices especially if the operational costs hinder the acquisition of data.

6. ACKNOWLEDGMENT

The work was made possible due to the Alfredo L. Juinio Professorial Chair Award. The author would like to acknowledge John Michael Tagle and Therese Rollan for their help in field operation and plotting, Julius Sempio for his statistical computation and Czar Jakiri Sarmiento and the Applied Geodesy and Space Technology (AGST) laboratory for the equipment. The author would also like to thank JulliaMacapinlac for her initial edits of the manuscript.

7. REFERENCES

1. Abeles, P. (2004). *BoofCV*. Retrieved June 15, 2012, from BoofCV: http://boofcv.org/index.php?title=Main_Page
2. Abeles, P. (2009). *Efficient Java Matrix Library*. Retrieved June 11, 2012, from efficient-java-matrix-library: <http://code.google.com/p/efficient-java-matrix-library/>
3. Armangué, X., & Salvi, J. (2003). Overall view regarding fundamental matrix estimation. *Image and Vision Computing* (21), 205-220.
4. Autodesk Inc. (2012). *Autodesk ImageModeler*. Retrieved August 15, 2012, from Autodesk: <http://usa.autodesk.com/adsk/servlet/pc/index?id=11390028&siteID=123112>
5. de By, R. A. (2001). *Principles of Geographic Information Systems*. ITC, Enschede, The Netherlands: ITC Educational Textbook Series.
6. DENR. (2007). *DENR Administrative Order No. 2007-29 - Revised Regulations on Land Survey*. Quezon City, Philippines: Department of Environment and Natural Resources.
7. EOS Systems Inc. (2012). *PhotoModeler*. Retrieved August 15, 2012, from PhotoModeler: <http://www.photomodeler.com>
8. Fusiello, A. (2000). Uncalibrated Euclidean reconstruction: a review. *Image and Vision Computing*, 555-563.

9. Hartley, R., & Zisserman, A. (2003). *Multiple View Geometry in Computer Vision*. United Kingdom: Cambridge University Press.
10. insight3d. (2009). *opensource image based 3d modeling software*. Retrieved August 15, 2012, from insight3d.
11. ISPRS. (2011, September 10). *Commission V - Close-Range Sensing: Analysis and Applications, 2008-2012*. Retrieved August 30, 2012, from International Society for Photogrammetry and Remote Sensing: http://research.ncl.ac.uk/pls/isprs_tcv/
12. Jiang, R., Jauregui, D. V., & White, K. R. (2008). Close-range photogrammetry applications in bridge measurement: Literature review. *Measurement* , 823-834.
13. LMB. (2011). *On Going Programs*. Retrieved August 15, 2012, from Department of Environment and Natural Resources, Land Management Bureau: http://lmb.gov.ph/On-Going_Programs.aspx
14. Plakas, K., & Trucco, E. (1998). Uncalibrated vision for 3-D underwater applications. *OCEANS'98 Conference* (pp. 272-276). Nice, France: IEEE/OS.
15. Salvi, J., Armangué, X., & Batlle, J. (2002). A comparative review of camera calibrating methods with accuracy evaluation. *Pattern Recognition* , 1617-1635.